

## MACROSCOPIC ELASTIC PROPERTIES OF PARTICLE MODELS

*Jan Stránský, Milan Jirásek and Václav Šmilauer*

Department of Mechanics, Faculty of Civil Engineering  
 Czech Technical University in Prague  
 Thákurova 7, 166 29 Prague  
 Czech Republic

(jan.stransky.1@fsv.cvut.cz, milan.jirasek@fsv.cvut.cz,  
 vaclav.smilauer@fsv.cvut.cz)

### ABSTRACT

Various forms of discrete models, such as lattice or particle models, are becoming increasingly popular in applications to highly nonlinear problems with large changes of the initial geometry. Such models consist of a finite number of "discrete elements" connected by links capturing all deformation processes, which are described by suitable constitutive equations formulated on the microscopic level. Parameters of these equations must be calibrated such that the entire model exhibits a realistic behavior on the macroscopic scale.

In this contribution, the relation between the elastic parameters governing the behavior of a single link and the resulting macroscopic elastic properties of particle models is investigated. The model considered here is three-dimensional, consisting of spherical rigid particles connected by interfaces that can transmit normal and shear stress. Calibration of the constitutive equations is simplified by dimensional analysis and is based on numerical simulations of a representative cell with periodic boundary conditions.

*Keywords:* Particle model, periodic cell, macroscopic properties, random packing, homogenization

### INTRODUCTION

Although the finite element method (FEM) is the most widely used tool for numerical analysis and computations across all engineering branches, other computational approaches (e.g. discrete models) can be useful in special cases.

Discrete models were originally developed for soil mechanics to simulate granular assemblies (Cundall and Strack, 1979), with individual grains modeled by particles. Since then, many different concepts and extensions of particle models appeared, e.g. beam-based lattice models (Schlangen and Garboczi, 1996), the discrete element method - DEM (Kun and Herrmann, 1996; Tavaréz and Plesha, 2007), as well as their applications, for example in simulations of fluid flow or analysis of macroscopically continuous cohesive-frictional materials like concrete.

In general, discrete models are composed of certain elementary units (building blocs, discrete elements) connected by deformable links. The elementary units can have the form of material points (with or without mass and inertia) or particles of finite size and specific shape, and are usually considered as perfectly rigid. All

deformation processes are then captured by the links (connections, interfaces) and depend on mutual displacement (or rotation) of connected elementary units. Using an appropriate constitutive law, the internal forces transmitted by each link are evaluated. According to the type of analysis, static equilibrium equations are solved (in static problems), or total forces acting on particles are evaluated and the equations of motion are integrated (in dynamic problems).

The constitutive laws can take various forms, from basic linear elasticity to linear or nonlinear viscosity, plasticity, damage etc. By their nature (modeling of a discontinuum), discrete models are suitable for highly discontinuous problems, such as crushing, massive cracking, impact problems etc. (Sawamoto et al., 1998; Liu et al., 2004).

### CONSIDERED PARTICLE MODEL

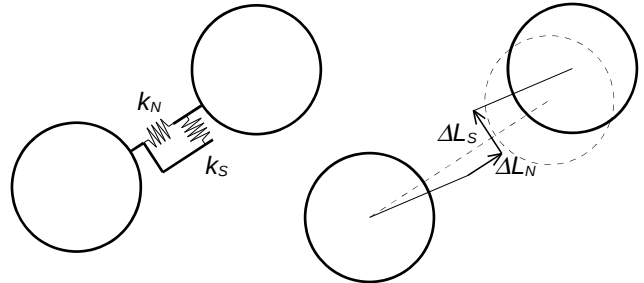


Fig. 1. 2D representation of contact stiffness (left) and contact displacement (right).

### Brief Description

The particle model investigated in this paper consists of rigid spheres with uniform radius  $R$  connected by links that can transmit normal stress and shear stress. The links connect centers of particles and can be represented by bars with length  $L$  and cross section area

$$A = \pi R^2 \quad (1)$$

Each particle possesses six degrees of freedom, three translations and three rotations. From the displacements of a connected couple of particles

$$\mathbf{u} = \{U_1, V_1, W_1, \phi_{1x}, \phi_{1y}, \phi_{1z}, U_2, V_2, W_2, \phi_{2x}, \phi_{2y}, \phi_{2z}\}^T$$

the relative contact displacements  $\Delta L_N$  and  $\Delta L_S$  and the equivalent strains

$\boldsymbol{\varepsilon} = \{\varepsilon_N, \boldsymbol{\varepsilon}_S\}^T = \{\Delta L_N, \Delta L_{S1}, \Delta L_{S2}\}^T/L$  can be evaluated. This kinematic relation is written in matrix form

$$\boldsymbol{\varepsilon} = \mathbf{B}\mathbf{u}, \quad (2)$$

where  $\mathbf{B}$  is the strain-displacement matrix.

The normal and shear contact (internal) forces  $F_N$  and  $\mathbf{F}_S$  are related to the normal and shear contact displacements  $\Delta L_N$  and  $\Delta \mathbf{L}_S$  through the elastic constitutive contact laws

$$F_N = \frac{Ak_N}{L} \Delta L_N \quad (3)$$

$$\mathbf{F}_S = \frac{Ak_S}{L} \Delta \mathbf{L}_S \quad (4)$$

in which  $k_N$  and  $k_S$  are the normal and shear contact stiffnesses; see Figure 1 for illustration.

Another important parameter of the model is the so-called interaction radius  $R_{int}$  that defines which particles are connected by links. The link between two particles is introduced if the distance between their centers,  $L$ , does not exceed  $2R_{int}$ . For  $R_{int}=R$ , only particles that are in direct contact are connected, which results into a rather loose internal structure.

### Micro-macro relationship of material parameters

In a cube of dimension  $C$  and volume  $V=C^3$  consider a random, densely packed assembly of spherical particles with radius  $R$ . If the number of particles  $N$  is high enough, the assembly behaves macroscopically as an isotropic material. The elastic properties of that material are determined by two material constants, for example Young's modulus  $E$  and Poisson ratio  $\nu$ .

In a very general case, we can express the macroscopic material properties as functions of all relevant variables:

$$E = f_E(k_N, k_S, R, R_{int}, C, N, A, L) \quad (5)$$

$$\nu = f_\nu(k_N, k_S, R, R_{int}, C, N, A, L). \quad (6)$$

Using dimensional analysis we can identify two dimensionally independent variables (e.g.  $k_N$  and  $R$ ) and one dimensionless variables  $N$ . Applying Buckingham  $\pi$  theorem, we can rewrite equations (5) and (6) in terms of new dimensionless variables as

$$\frac{E}{k_N} = \pi_E \left( \frac{k_S}{k_N}, \frac{R^2}{A}, \frac{R}{C}, \frac{R_{int}}{R}, N \right), \quad (7)$$

$$\nu = \pi_\nu \left( \frac{k_S}{k_N}, \frac{R^2}{A}, \frac{R}{C}, \frac{R_{int}}{R}, N \right). \quad (8)$$

Based on physical considerations, most of the dimensionless variables on the right side of (7) and (8) can be eliminated.

In principle, the number of particles  $N$  could be considered as independent of the relative particle size  $R/C$ . However, we are interested in the behavior of densely packed assemblies of particles, which are prepared by a simulated compaction process. It turns out that, for large values of  $N$ , the packing fraction  $4\pi NR^3/3C^3$  tends to a constant, approximately equal to 0.625, which is close to the value 0.64 (theoretical

maximum packing fraction for random close packing (Torquato et al., 2000)); see Figure 2. Therefore, the ratio  $R/C$  for such dense assemblies can be determined from  $N$  and does not need to be considered as an independent variable.

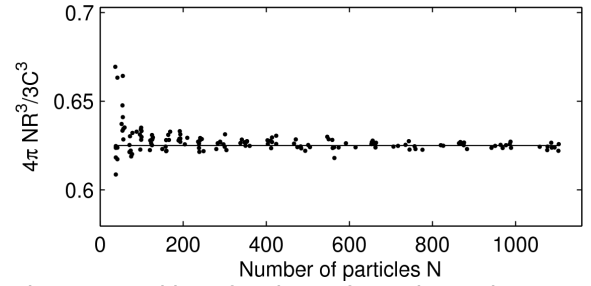


Fig. 2. Packing fraction of random close packed assemblies for varying  $N$ .

Furthermore, as  $N$  tends to infinity, the macroscopic properties approach a certain limit, which represents the effective properties of an equivalent elastic continuum. If it is chosen sufficiently high, the corresponding periodic cell is a representative volume element and its properties are close to the theoretical limit. Therefore,  $N$  does not need to be considered as a variable influencing the results, it just has to be chosen sufficiently high.

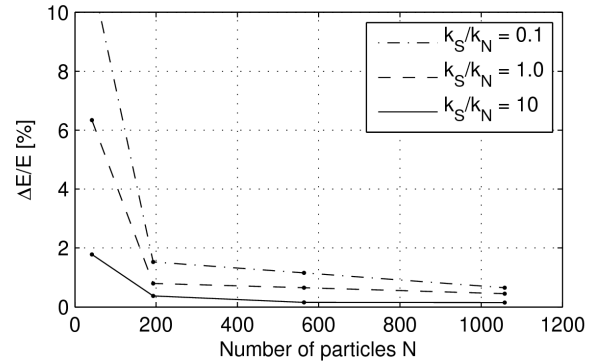


Fig. 3. Relative anisotropy of Young's modulus  $\Delta E/E$  (see equation (25)) for  $R_{int}/R = 1.6$  for varying  $N$ .

The ratio  $R^2/A$  is taken as constant, according to equation (1). Even if it was not, the dependence of the macroscopic properties on this ratio would be very simple. Young's modulus (or any other elastic stiffness) would be inversely proportional to  $R^2/A$  and the Poisson ratio would not depend on it at all.

After all these considerations, we can rewrite the relationship between macro- and microscopic material parameters as

$$\frac{E}{k_N} = \pi_E \left( \frac{k_S}{k_N}, \frac{R_{int}}{R} \right), \quad (9)$$

$$\nu = \pi_\nu \left( \frac{k_S}{k_N}, \frac{R_{int}}{R} \right). \quad (10)$$

### Theoretical analytical solution

In analogy to microplane models, an analytical derivation of tensor of macroscopic elastic stiffness  $\mathbf{D}_e$  presented by Kuhl et al. (2001) yields

$$\mathbf{D}_e = \frac{1}{V} \sum_c A L_c (k_N \mathbf{N}_c \otimes \mathbf{N}_c + k_S \mathbf{T}_c^T \cdot \mathbf{T}_c), \quad (11)$$

where  $c$  is a subscript identifying individual links, the sum is taken over all links in the cell.  $\mathbf{N}$  and  $\mathbf{T}$  are projection tensors given by

$$\mathbf{N} = \mathbf{n} \otimes \mathbf{n}, \quad (12)$$

$$\mathbf{T} = \mathbf{n} \cdot \mathbf{I}_S - \mathbf{n} \otimes \mathbf{n} \otimes \mathbf{n}, \quad (13)$$

where  $\mathbf{n}$  is a unit vector specifying the direction of the link,  $\mathbf{I}_S$  is the symmetric fourth-order unit tensor ( $I_{ijkl}^S = [\delta_{ik}\delta_{jl} + \delta_{il}\delta_{jk}]/2$ ),  $\delta_{ij}$  is the Kronecker delta. Under the assumption that the links are distributed with uniform probability over all possible directions, the following expression can be derived (see Kuhl et al., 2001, for more details):

$$\begin{aligned} \mathbf{D}_e &= \frac{A \sum_c L_c}{4\pi V} \int_{\Omega} (k_N \mathbf{N}_c \otimes \mathbf{N}_c + k_S \mathbf{T}_c^T \cdot \mathbf{T}_c) d\Omega = \\ &= \frac{A \sum_c L_c}{5V} (k_N - k_S) \mathbf{I}_V + \frac{A \sum_c L_c}{15V} (2k_N + 3k_S) \mathbf{I}_S, \end{aligned} \quad (14)$$

Here,  $\mathbf{I}_V$  is the fourth-order volumetric projection tensor ( $I_{ijkl}^V = 1/3 \delta_{ij}\delta_{kl}$ ). Comparing equations (14) with the elastic isotropic stiffness tensor

$$\mathbf{D}_e = \frac{3E\nu}{(1+\nu)(1-2\nu)} \mathbf{I}_V + \frac{E}{1+\nu} \mathbf{I}_S, \quad (15)$$

we can write the final relation between macroscopic material properties  $E$  and  $\nu$  and microscopic model parameters  $k_N$  and  $k_S$  as

$$\nu = \frac{k_N - k_S}{4k_N + k_S} \quad (16)$$

$$\frac{E}{k_N} = \frac{A \sum_c L_c}{3V} \frac{2 + 3 \frac{k_S}{k_N}}{4 + \frac{k_S}{k_N}}. \quad (17)$$

## NUMERICAL SIMULATIONS

Numerical analyses have been performed for a number of randomly generated periodic particle assemblies. These assemblies have been prepared by a compaction process simulated using the open-source discrete element code YADE (Šmilauer, 2010). For the actual analysis, however, the finite element solver OOFEM (Patzák and Bittnar, 2001) has been used. This code allows a direct solution of the static equilibrium equations, which is faster than dynamic discrete element analysis performed with YADE, with inertial effects gradually removed by damping. Even though OOFEM is a framework for the finite element method, discrete elements can be easily implemented as a “pseudo-truss” structure, in which particles and links of the discrete model are considered as special nodes and elements of the finite element model. Of course, the present elastic static problem is not a typical case in which DEM would be used. However, this step is necessary for calibrating the aforementioned microscopic parameters of the model, to be used in more complicated problems, for instance those that involve impact and fragmentation.

The implementation of the model into the finite element solver OOFEM consisted in defining special elements representing links. In this context, we would like to emphasize the advantages provided by the object-oriented architecture of OOFEM.

The FEM analysis of such particle model is based on equations (2), (3) and (4). By combining these equations, the stiffness matrix of element number  $e$  takes the form

$$\mathbf{K}^e = \mathbf{L} \mathbf{B}^T \mathbf{D} \mathbf{B}, \quad (18)$$

where

$$\mathbf{D} = \begin{bmatrix} k_N & 0 & 0 \\ 0 & k_S & 0 \\ 0 & 0 & k_S \end{bmatrix}. \quad (19)$$

is the material stiffness matrix of the element.

## Periodic boundary conditions

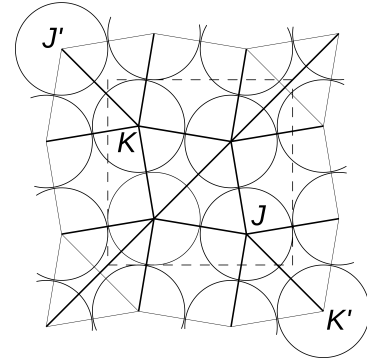


Fig. 4. 2D example of periodic cell and “periodic” links.

Numerical simulations have been done on a representative cell with periodic boundary conditions. The implementation of the periodic boundary conditions is analogous to the implementation described by Grassl and Jirásek (2010). Elements crossing the boundary of the bounding cube (connecting one particle inside the cell with another particle physically located in one of the neighboring cells) is modified in a special way. Consider such an element connecting particles  $J'$  and  $K$  and a corresponding element connecting periodic images of these particles, denoted as  $J$  and  $K'$  (see Figure 4). Both elements are real links of the structure, but for the analysis purposes only one of them is taken into account when setting up the equilibrium equations (in our example we chose link  $JK'$ ). Periodic boundary conditions are imposed by the set of constraint equations that contain the components of macroscopic deformation  $\mathbf{E} = \{E_x, E_y, E_z, E_{yz}, E_{zx}, E_{xy}\}^T$ :

$$\begin{aligned} u_{K'} &= u_K + E_x k_x C + E_{xy} k_y C \\ v_{K'} &= v_K + E_y k_y C + E_{yz} k_z C \\ w_{K'} &= w_K + E_z k_z C + E_{zx} k_x C \\ \phi_{xK'} &= \phi_{xK} \\ \phi_{yK'} &= \phi_{yK} \\ \phi_{zK'} &= \phi_{zK}. \end{aligned} \quad (20)$$

$C$  is the dimension of the cubic periodic cell, constants  $k$  have values -1, 0 or 1 and specify the position of the particle outside the cell according to the relations

$$\begin{aligned} x_{K'} &= x_k + k_x C \\ y_{K'} &= y_k + k_y C \\ z_{K'} &= z_k + k_z C. \end{aligned} \quad (21)$$

Using equations (20) and (21), the displacement of connected particles  $K$  and  $J'$  (periodic image of particle  $J$ ) can be written in terms of the displacements of particles  $J$  and  $K$  and the macroscopic deformation as

$$\begin{pmatrix} \mathbf{u}_{K'} \\ \mathbf{u}_{J'} \end{pmatrix} = \mathbf{T} \begin{pmatrix} \mathbf{u}_K \\ \mathbf{u}_J \\ \mathbf{E} \end{pmatrix}. \quad (22)$$

The upper block (first 12x12 components out of 18x12) of the transformation matrix  $\mathbf{T}$  corresponds to the identity matrix, and the only non-zero components of the lower block are in rows 7-9 and in columns 13-18:

$$\mathbf{T}_{(7-9;13-18)} = \begin{matrix} & \begin{matrix} 13 & 14 & 15 & 16 & 17 & 18 \end{matrix} \\ \begin{matrix} 7 \\ 8 \\ 9 \end{matrix} & \begin{bmatrix} k_x C & 0 & 0 & 0 & 0 & k_y C \\ 0 & k_y C & 0 & k_z C & 0 & 0 \\ 0 & 0 & k_z C & 0 & k_x C & 0 \end{bmatrix} \end{matrix} \quad (23)$$

Using the transformation matrix  $\mathbf{T}$ , the modified stiffness matrix of the “periodic” elements (with 18 rows and 18 columns) can be expressed in the form

$$\mathbf{K}^e = \mathbf{L} \mathbf{T}^T \mathbf{B}^T \mathbf{D} \mathbf{B} \mathbf{T}. \quad (24)$$

The components of macroscopic deformation  $\mathbf{E}$  are therefore considered as global degrees of freedom. The corresponding “load” components are directly related to the macroscopic stress (they are equal to the stress components multiplied by the volume of the cell).

To prevent displacement of the assembly as a rigid body, one particle need to be “supported” by setting its three displacements to zero.

### Computations

Several particle assemblies have been analyzed and the macroscopic constants  $E$  and  $\nu$  have been evaluated for a number of values of the dimensionless ratios  $R_{\text{int}}/R$  and  $k_S/k_N$ .

For each assembly, six simulations have been performed. In each simulation, one component of the macroscopic deformation  $\mathbf{E}$  has been set to one while all the others have been prescribed as zeros. The individual components of the macroscopic stress then represent the coefficients in one column of the macroscopic stiffness matrix  $\mathbf{D}_e$ .

The resulting material is first considered as orthotropic, with compliance matrix  $\mathbf{C}_e$  (25), from which material parameters  $E_1, E_2, E_3, \nu_{12}, \nu_{21}, \nu_{13}, \nu_{31}, \nu_{23}, \nu_{32}$  are easily extracted. In the ideal case of an isotropic material, all Young's moduli and Poisson ratios would be identical. To verify that the results indeed closely correspond to an isotropic behavior is one of the goals of this paper.

$$\mathbf{C}_e = (\mathbf{D}_e)^{-1} = \begin{bmatrix} \frac{1}{E_1} & -\frac{\nu_{21}}{E_2} & -\frac{\nu_{31}}{E_3} & 0 & 0 & 0 \\ -\frac{\nu_{12}}{E_1} & \frac{1}{E_2} & -\frac{\nu_{32}}{E_3} & 0 & 0 & 0 \\ -\frac{\nu_{31}}{E_1} & -\frac{\nu_{32}}{E_2} & \frac{1}{E_3} & 0 & 0 & 0 \\ 0 & 0 & 0 & \frac{1}{G_{23}} & 0 & 0 \\ 0 & 0 & 0 & 0 & \frac{1}{G_{31}} & 0 \\ 0 & 0 & 0 & 0 & 0 & \frac{1}{G_{12}} \end{bmatrix} \quad (25)$$

To introduce an objective measure, the “relative anisotropy” of macroscopic Young's modulus

$$\Delta E/E = \frac{\max_i \{|E_i - E_{\text{mean}}|\}}{E_{\text{mean}}} \quad (26)$$

is defined. The dependence of the relative anisotropy on the number of particles (and thus on the size of the cell) is shown in Figure 3. As expected, with increasing number of particles the deviation of the moduli from isotropy diminishes.

In a similar way, the relative anisotropy of Poisson ratio

$$\Delta \nu/\nu = \frac{\max_{ij} \{|\nu_{ij} - \nu_{\text{mean}}|\}}{\nu_{\text{mean}}}, \quad (27)$$

and of the shear modulus

$$\Delta G/G = \frac{\max_i \{|G_i - E_{\text{mean}}/2(1 + \nu_{\text{mean}})|\}}{E_{\text{mean}}/2(1 + \nu_{\text{mean}})} \quad (28)$$

have been defined. Also, a measure of the deviation of those components of the stiffness matrix that should vanish has been defined as

$$\Delta/E = \frac{\max_{ij} \{D_{ij}\}}{E_{\text{mean}}}. \quad (29)$$

## RESULTS AND DISCUSSION

Firstly, macroscopic isotropy and stability of results for a variable number of particles  $N$  has been studied. The findings can be summarized as:

- The mean material parameters  $E$  and  $\nu$  are almost independent on the number of particles, even for  $N$  less than 100. For more than 200 particles per periodic cell, the values of mean material parameters do not change for any type of simulation (i.e., for any ratio  $k_S/k_N$  and any interaction radius  $R_{\text{int}}$ ).
- The relative anisotropy of Young's modulus decreases with increasing number of particles. The convergence is faster for higher  $R_{\text{int}}/R$  and for higher  $k_S/k_N$ .
- The relative anisotropy of Poisson ratio  $\nu$  has a similar trend: for an increasing number of particles its relative anisotropy decreases. In contrast to the case of Young's modulus, the slowest (or even no convergence at all) has been observed for ratio  $k_S/k_N$  close to 1. This is caused by the fact that for  $k_S/k_N=1$  the Poisson ratio  $\nu$  has a theoretical value 0 and the relative error is therefore higher.

- The theoretically vanishing components of the stiffness matrix of the macroscopic material are indeed almost zero, again for increasing  $N$  the error is smaller. Faster convergence has been observed on samples with higher  $R_{int}/R$  and for  $k_S/k_N$  closer to 1.
- The relative error of the formula  $G = E/2(1+\nu)$  gets smaller for increasing  $N$ . The convergence is faster for  $k_S/k_N$  closer to 1.
- All of the general trends described above are consistent with our expectations.

Secondly, the relation between the micro- and macroscopic material parameters has been observed. The mean values of parameters have been considered as the numerical results. The numerical relation between macro- and microscopic parameters has been constructed for several values of  $R_{int}/R$  and compared to the theoretical values. In graphs, points represent numerically obtained data and lines represent the theoretical dependence.

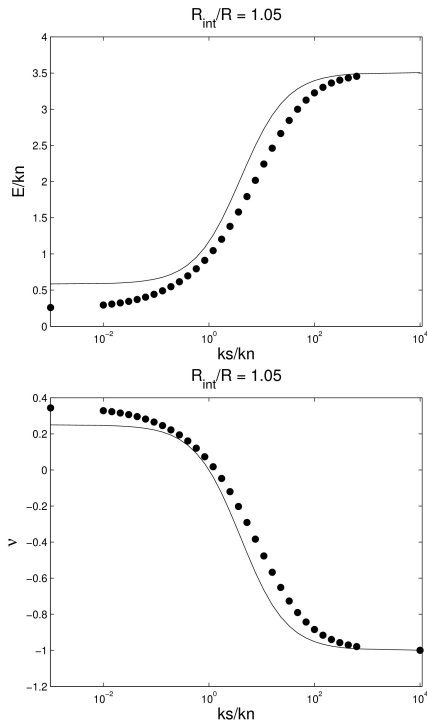


Fig. 5. Relation between macro- and microscopic parameters for  $R_{int}/R= 1.05$  (semilogarithmic plot).

As seen from the graphs, the agreement between theoretically and numerically obtained data is very good for higher  $R_{int}/R$ . On the other hand, the theoretical formula underestimates the actual (numerically determined) values of Poisson ratio and overestimates the actual values of Young's modulus for  $R_{int}/R < 1.3$ .

For all values of  $R_{int}/R$ , the value of Poisson ratio in the limit case for  $k_S/k_N \rightarrow \infty$  ( $k_N = 0$ ) is -1 (extreme theoretical value for Poisson ratio), while the maximum attainable value is 1/4 for higher  $R_{int}/R$ , which corresponds to equation (16). A higher value, up to 0.343, is obtained for  $R_{int}/R = 1.05$ .

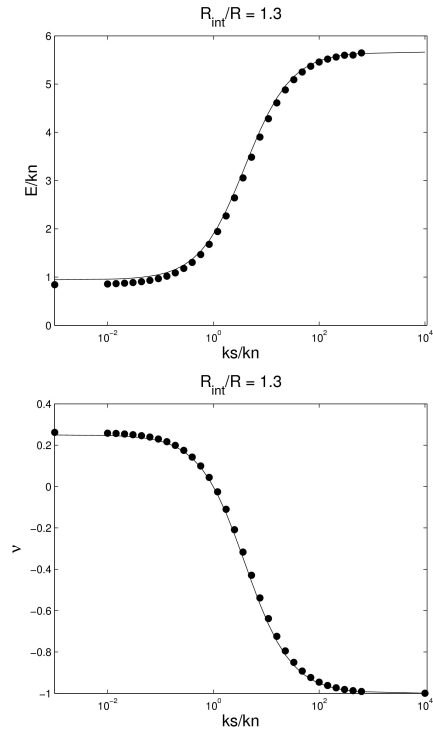


Fig. 6. Relation between macro- and microscopic parameters for  $R_{int}/R= 1.3$  (semilogarithmic plot).

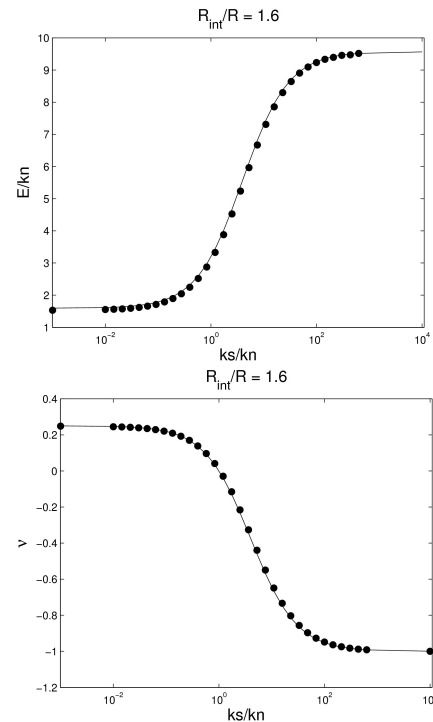


Fig. 7. Relation between macro- and microscopic parameters for  $R_{int}/R= 1.6$  (semilogarithmic plot).

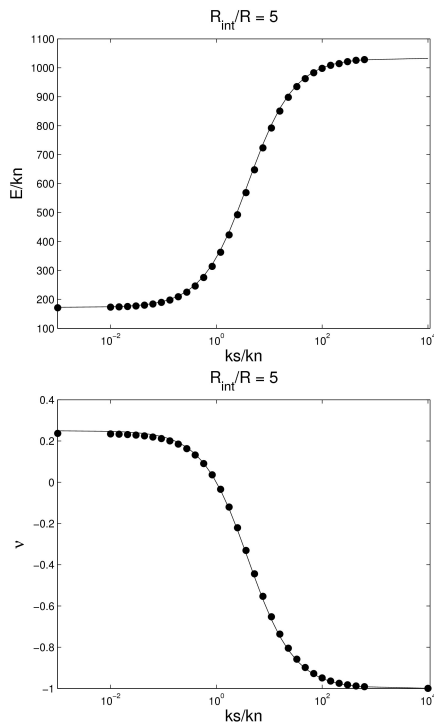


Fig. 8. Relation between macro- and microscopic parameters for  $R_{int}/R=5.0$  (semilogarithmic plot).

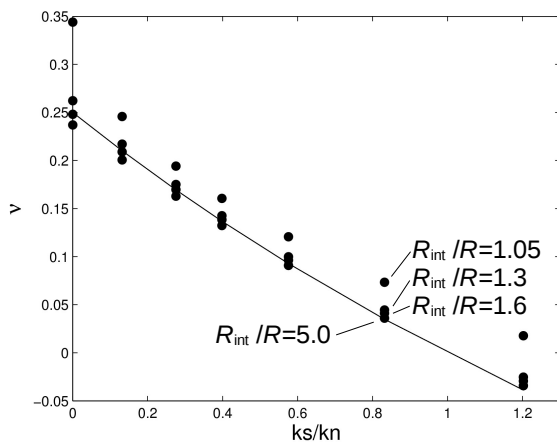


Fig. 9. Relation between Poisson ratio and microscopic parameters for all investigated values  $R_{int}/R$ .

## CONCLUSIONS

A particle model consisting of randomly placed and densely packed rigid spheres connected by deformable linear elastic links has been investigated in this paper. It has been proven that such a random assembly behaves macroscopically as an isotropic material and deviations from the isotropy decrease with increasing number of particles of the assembly. The convergence is faster for a higher interaction radius.

The relationship between microscopic parameters of individual links and effective properties of the macroscopic material has been investigated both numerically and analytically. A good agreement between analytical and numerical results has been found for high interaction radii, while for interaction radius less than 1.3 times the particle radius the theoretical formula underestimates Poisson ratio and overestimates Young's modulus.

## Acknowledgement

Financial support of the Czech Science Foundation under project GAČR 106/08/1508 is gratefully acknowledged.

## REFERENCES

1. P. Cundall, O. Strack, "A discrete numerical model for granular assemblies", *Geotechnique*, vol. 29, no. 1, pp. 47-65, 1979.
2. E. Schlangen, E. J. Garboczi, "New method for simulating fracture using an elastically uniform random geometry lattice", *International Journal of Engineering Science*, vol. 34, no. 10, pp. 1131-1144, 1996.
3. F. Kun, H. J. Herrmann, "A study of fragmentation processes using a discrete element method", *Computational Methods in Applied Mechanics and Engineering*, vol. 138, pp. 3-18, 1996.
4. F. A. Tavarez, M. E. Plesha, "Discrete element method for modelling solid and particulate materials", *International Journal for Numerical Methods in Engineering*, vol. 70, pp. 379-404, 2007.
5. Y. Sawamoto, H. Tsubota, Y. Kasai, N. Koshika, H. Morikawa, "Analytical studies on local damage to reinforced concrete structures under impact loading by discrete element method", *Nuclear engineering and Design*, vol. 179, pp. 157-177, 1998.
6. K. Liu, L. Gao, S. Tanimura, "Application of Discrete Element Method in Impact Problems", *Japan Society Mechanical Engineering*, vol. 47, no. 2, pp. 138-145, 2004.
7. S. Torquato, T. M. Truskett, P.G. Debenedetti, "Is random close packing of spheres well defined?", *Physical Review Letters*, vol. 84, no. 10, pp. 2064-2067, 2000.
8. E. Kuhl, G. A. D'Addetta, M. Leukart, E. Ramm, "Microplane modelling and particle modelling of cohesive-frictional materials", 2001.
9. V. Šmilauer, (12.3.2010), *Yade: past, present, future*, Retrieved from <https://yade-dem.org/images/5/59/Eudoxos2010-yade-past-present-future.pdf>.
10. B. Patzák, Z. Bittnar, "Design of object oriented finite element code", *Advances of Engineering Software*, vol. 32, pp. 759-767, 2001.
11. P. Grassl, M. Jirásek, "Meso-scale approach to modelling the fracture process zone of concrete subjected to uniaxial tension", *International Journal of Solids and Structures*, vol. 47, pp. 957-968, 2010.